Non-linear mechanical behavior of the elastomer polydimethylsiloxane (PDMS) used in the manufacture of microfluidic devices

R. C. HUANG and L. ANAND
Department of Mechanical Engineering
Massachusetts Institute of Technology
Cambridge, MA 02139, USA

***Abstract*— Polydimethylsiloxane (PDMS) is the elastomer of choice to create a variety of microfluidic devices by soft lithography techniques (e.g., [1], [2], [3], [4]). Accurate and reliable design, manufacture, and operation of microfluidic devices made from PDMS, require a detailed characterization of the deformation and failure behavior of the material. This paper discusses progress in a recently-initiated research project towards this goal. We have conducted large-deformation tension and compression experiments on traditional macroscale specimens, as well as microscale tension experiments on thin-film ($\approx 50\mu$m thickness) specimens of PDMS with varying ratios of monomer:curing agent (5:1, 10:1, 20:1). *We find that the stress-stretch response of these materials shows significant variability, even for nominally identically prepared specimens*.**

A non-linear, large-deformation rubber-elasticity model [5], [6] is applied to represent the behavior of PDMS. The constitutive model has been implemented in a finite-element program [7] to aid the design of microfluidic devices made from this material.

As a first attempt towards the goal of estimating the non-linear material parameters for PDMS from indentation experiments, we have conducted micro-indentation experiments using a spherical indenter-tip, and carried out corresponding numerical simulations to verify how well the numerically-predicted P (load-h (depth of indentation) curves compare with the corresponding experimental measurements. The results are encouraging, and show the possibility of estimating the material parameters for PDMS from relatively simple micro-indentation experiments, and corresponding numerical simulations.

***Index Terms*— Microfluidics, PDMS, elastomers, hyperelasticity, micro-indentation.**

I. Introduction

MICROFLUIDIC devices are microsystems which control the flow of small volumes (nano- or pico-liters) of fluids (gases or liquids) through micro-capillary channels on a "chip" which is integrated with computerized analytical instruments. Such devices contain active and passive microstructural features that control the flow and mixing of the fluids to produce physical, chemical and microbiological reactions on small volumes of materials, and are beginning to be used in a wide variety of applications: e.g., biochemical assays, capillary electrophoresis, cell counting and sorting, cell growth, detection of biological species, genomics, liquid chromatography, and even computation.

Unlike the field of micro-electro-mechanical systems (MEMS), for which the material of choice has long been silicon, and for which the microfabrication techniques have been borrowed from the well-established microelectronics industry, the materials of choice for microfluidic systems are the optically-transparent materials: (a) glass or quartz, (b) amorphous glassy polymers (e.g., polymethylmethacrylate, PMMA, polycarbonate, PC), and (c) elastomeric polymers (e.g., polydimethylsiloxane, PDMS).

Glasses have good properties, which include well-defined surface chemistries, superior optical characteristics and good electro-osmotic properties. However, these materials present a number of issues (e.g., low aspect ratio of etched-microstructures, high temperatures required for bonding multi-layered devices, and relatively high cost) that will hinder their widespread use in commercial manufacture of microfluidic devices. In contrast, amorphous glassy polymers (e.g., PMMA, PC) and elastomeric polymers (e.g., PDMS) provide for a wide range of material properties, are available in pure forms at low cost, and can be machined and replicated in a variety of manners. These qualities have generated enormous interest in the development of manufacturing processes for polymeric microfluidic devices for numerous applications.

There are a variety of potential methods available for manufacturing polymeric substrates for microfluidic applications. Of emerging importance are replication methods such as hot-embossing for amorphous thermoplastic materials, and soft-lithography for elastomeric materials. These processes involve the use of a precision

L. Anand is an SMA-IMST Fellow; E-mail:anand@mit.edu

template or master-mold from which many identical polymer microstructures can be made.

In this paper we focus on soft-lithography [2], which has become a highly popular replication process over the past five years. It offers a rapid, flexible and cost-effective manufacturing route for the creation of micron-sized features on planar substrates in elastomeric siloxane polymers, e.g. PDMS. The elastomer PDMS has several characteristics that make it ideal for microfluidic devices [1]: e.g., (a) It is easily molded to conform and replicate feature sizes of less than 0.1 micron. (b) Because of its low surface free energy, it can be lifted easily from molds and reversibly sealed to other materials. (c) It is non-toxic and can support cell growth. (d) It is permeable to gases and non-polar organic solvents, but is impermeable to liquid water. (e) It is optically transparent and has a UV cutoff of 240 nm and optical detection from 240 to 1100 nm. (f) It is electrically insulating which allows for embedded circuits.

Laboratory-prototype microfluidic devices made from PDMS have been developed for numerous applications such as biochemical assays, capillary electrophoresis and cell growth, as well as cell counting and sorting (cf., e.g., [3], [4]). Commercial scale manufacture of microfluidic devices is just beginning.[1]

Accurate and reliable design, manufacture, and operation of microfluidic devices made from PDMS require: (a) a detailed characterization of the deformation and failure behavior of PDMS; (b) an understanding and modelling of the interfacial decohesion of PDMS from a substrate to facilitate demolding; (c) an optimization of geometries of the device components, such as layer thicknesses and channel dimensions; (d) an optimization of flow characteristics within the channels; (e) a specification of safe operating parameters; and (f) the prevention of interface-decohesion and fatigue failures, so that the devices properly and reliably serve their intended functions.

This paper summarizes progress on a recently-initiated research project on the characterization of the deformation and failure behavior of PDMS. We begin by reviewing a non-linear, large deformation rubber-elasticity model in Section II [5], [6]. Section III describes our macroscale tension and compression experiments on PDMS. The applicability of the non-linear rubber-elasticity model to represent the behavior of PDMS is explored in Section IV. Section V summarizes the applicability of the model to represent the tensile stress-stretch behavior of thin-film microscale specimens.

As a first attempt towards the goal of estimating the non-linear material parameters for PDMS from indentation experiments, we have conducted micro-indentation experiments using a spherical indenter tip, and carried out corresponding finite element simulations[2] to verify how well the numerically-predicted load P (load)-h (depth of indentation) curves compare with the corresponding experimental measurements; these results are presented in Section VI. The results are encouraging, and show the possibility of estimating the material parameters for PDMS from relatively simple micro-indentation experiments, and corresponding numerical simulations.

The paper ends with some concluding remarks in Section VII.

II. A NON-LINEAR RUBBER-ELASTICITY MODEL

The internal structure of elastomeric solids consists of a three-dimensional macromolecular network in which flexible macromolecules are connected at junction points provided by chemical cross-links between the macromolecules. A chain is defined as the segment of a macromolecule between junction points. Each chain is flexible and contains more or less freely-jointed rigid links. In the absence of any imposed deformation the freely-jointed links in each chain cause the chain to take a randomly- kinked form because of the thermal agitation of the atoms in the chain. Upon the application and release of a stress, the molecules quickly revert to their normal crumpled form in the unstressed configuration, and this **change in entropy** is the basis of the reversible high extensibility of elastomeric solids.

A. Kinematics

Consider a rectangular parallelopiped volume element with edge lengths dX_1, dX_2, dX_3 in the reference configuration aligned with a Cartesian coordinate system with base vectors $\{\mathbf{e}_i | i = 1, 2, 3\}$; cf. Fig.1 (a). The elemental volume of the parallelopiped is

$$dv_0 = dX_1\, dX_2\, dX_3\,. \tag{1}$$

Consider a deformation in which the elemental volume is still a rectangular parallelopiped, but with edge lengths dx_1, dx_2, dx_3, and volume

$$dv = dx_1\, dx_2\, dx_3\,. \tag{2}$$

The ratios, λ_i, defined by

$$\lambda_1 \stackrel{\text{def}}{=} \frac{dx_1}{dX_1}, \qquad \lambda_2 \stackrel{\text{def}}{=} \frac{dx_2}{dX_2}, \qquad \lambda_3 \stackrel{\text{def}}{=} \frac{dx_3}{dX_3}, \tag{3}$$

[1] For example, Fluidigm (http://www.fluidigm.com). Fluidigm's approach is to produce elastomeric chips in which microscale valves and pumps are integrated into a chip using multi-layer soft lithography. The chips contain "active plumbing" in the form of on-chip valves and peristaltic pumps. Each layer of the Fluidigm chip is separately micro cast and then bonded to its neighboring layers to form a monolithic elastomeric structure containing a three-dimensional network of channels.

[2] We have implemented a compressible version of the the rubber-elasticity constitutive model [6] in the finite-element program Abaqus/Explicit [7].

are called *stretch-ratios*. Hence, the volume ratio, denoted by J is

$$J \stackrel{\text{def}}{=} \frac{dv}{dv_0} = \lambda_1\lambda_2\lambda_3\,. \tag{4}$$

An important characteristic of rubber-like materials such as PDMS is that they are *almost incompressible*. For simplicity we shall assume that the kinematical response of PDMS is *completely incompressible*:

$$J = \lambda_1\lambda_2\lambda_3 = 1. \tag{5}$$

B. Engineering stresses. Rate of work per unit reference volume

Let $\dot{\overline{dx_i}}$ be the rates of change of the elemental lengths dx_i, and let f_i, be the corresponding power-conjugate forces; see Fig. 1 (b). Thus the *rate of work per unit reference volume* performed in deforming the elemental volume is

$$\dot{w} \stackrel{\text{def}}{=} \sum_{i=1}^{3} S_i\dot{\lambda}_i\,. \tag{6}$$

where the stretch rates are

$$\dot{\lambda}_1 = \frac{\dot{\overline{dx_1}}}{dX_1}, \qquad \dot{\lambda}_2 = \frac{\dot{\overline{dx_2}}}{dX_2}, \qquad \dot{\lambda}_3 = \frac{\dot{\overline{dx_3}}}{dX_3}, \tag{7}$$

and the corresponding power-conjugate *engineering stresses* are

$$S_1 = \frac{f_1}{dX_2dX_3}, \quad S_2 = \frac{f_2}{dX_1dX_3}, \quad S_3 = \frac{f_3}{dX_1dX_2}. \tag{8}$$

C. Rate of change of free energy. Free energy balance for an elastic material

Let ψ be the free-energy density per unit reference volume of the material. Then, in general, the rate of change of the free energy has to be less than the rate of work performed in deforming the elemental volume (second law of thermodynamics under isothermal conditions):

$$\dot{\psi} \le \dot{w}. \tag{9}$$

For an *elastic material*, that is for a material which shows no disspation, the rate of change in the free energy is *equal* to the rate of work:

$$\dot{\psi} = \dot{w}\,. \tag{10}$$

D. Free energy density for an isotropic, incompressible rubber-elastic material

We consider a free-energy function, which is a symmetric function of the principal stretches $\lambda_i\,(i = 1, 2, 3)$:

$$\psi = \hat{\psi}(\lambda_1, \lambda_2, \lambda_3)\,. \tag{11}$$

In an ideally incompressible material the volume ratio $J = \lambda_1\lambda_2\lambda_3$ satisfies the constraint

$$J - 1 = 0. \tag{12}$$

For an incompressible material the free energy is unaltered if we modify the free-energy function (11) as follows:

$$\psi = \hat{\psi}(\lambda_1, \lambda_2, \lambda_3) - \underbrace{\underbrace{p}_{\text{arbitrary pressure}} \times \underbrace{(J-1)}_{\text{Incompressibility constraint}}}_{=0} \tag{13}$$

In physical terms, the quantity p represents an *arbitrary pressure* necessary to maintain the constraint $J - 1 = 0$. Thus, *in an incompressible material the free energy is unaltered by an arbitrary hydrostatic pressure*. This pressure is "arbitrary" only in the sense that it does not effect the free energy. As we shall see shortly, in actual physical situations traction boundary conditions serve to determine p in a physical problem.

E. Consequences of free-energy balance for an elastic material

In order to apply the balance (10), we need to calculate $\dot{\psi}$:

$$\dot{\psi} = \sum_{i=1}^{3} \frac{\partial\hat{\psi}(\lambda_1, \lambda_2, \lambda_3)}{\partial\lambda_i}\,\dot{\lambda}_i - p\dot{J}\,. \tag{14}$$

Since,

$$\dot{J} = \sum_{i=1}^{3} \lambda_i^{-1}\dot{\lambda}_i\,, \tag{15}$$

substituting this in (14) gives

$$\dot{\psi} = \sum_{i=1}^{3} \left\{ \frac{\partial\hat{\psi}(\lambda_1, \lambda_2, \lambda_3)}{\partial\lambda_i} - p\lambda_i^{-1} \right\} \dot{\lambda}_i\,. \tag{16}$$

Thus, substituting (16) and (6) into (10) we obtain

$$\sum_{i=1}^{3} \left\{ \left(\frac{\partial\hat{\psi}(\lambda_1, \lambda_2, \lambda_3)}{\partial\lambda_i} - p\lambda_i^{-1} \right) - S_i \right\} \dot{\lambda}_i = 0\,. \tag{17}$$

This equality is satisfied for all $\dot{\lambda}_i$ only if

$$S_i = \frac{\partial\hat{\psi}(\lambda_1, \lambda_2, \lambda_3)}{\partial\lambda_i} - p\lambda_i^{-1}, \tag{18}$$

which gives the relation for the engineering stress in terms of the principal stretches, for an isotropic, incompressible, non-linear hyperelastic material.

F. Specialization of the free-energy function

Let

$$\bar{\lambda} \stackrel{\text{def}}{=} \frac{1}{\sqrt{3}}\sqrt{\lambda_1^2+\lambda_2^2+\lambda_3^2} \tag{19}$$

define an **effective stretch**. We consider a special free-energy function which depends only on the *effective stretch* [5], [6]:

$$\hat{\psi}(\bar{\lambda}), \qquad \text{with} \qquad \hat{\psi}(1)=0. \tag{20}$$

In this case,

$$\frac{\partial \hat{\psi}(\bar{\lambda})}{\partial \lambda_i} = \mu\,\lambda_i \tag{21}$$

where

$$\boxed{\mu \stackrel{\text{def}}{=} \left(\frac{1}{3\bar{\lambda}}\,\frac{\partial \hat{\psi}(\bar{\lambda})}{\partial \bar{\lambda}}\right)} \tag{22}$$

is a *generalized shear modulus*. Hence, using (21) and (22), the equation for the engineering stresses (18) becomes

$$\boxed{S_i = \mu\lambda_i - p\lambda_i^{-1}}\,. \tag{23}$$

In elastomeric materials the major part of ψ arises from an "entropic" contribution. Based on statistical mechanics models of rubber elasticity we consider the *Langevin-inverse* form

$$\begin{aligned}\psi = \mu_R\,\lambda_L^2\,\Bigg[&\left(\frac{\bar{\lambda}}{\lambda_L}\right)\,x + \ln\left(\frac{x}{\sinh x}\right)\\ &-\left(\frac{1}{\lambda_L}\right)\,y - \ln\left(\frac{y}{\sinh y}\right)\Bigg],\\ x=\mathcal{L}^{-1}\left(\frac{\bar{\lambda}}{\lambda_L}\right), &\qquad y=\mathcal{L}^{-1}\left(\frac{1}{\lambda_L}\right),\end{aligned} \tag{24}$$

where $\mathcal{L}^{-1}$ is the inverse[3] of the Langevin function $\mathcal{L}(\cdots)=\coth(\cdots)-(\cdots)^{-1}$. This functional form for ψ involves two material parameters:

> μ_R, called the *rubbery modulus*, and λ_L called the *network locking stretch*.

In this case, from (22), the shear modulus is

$$\mu = \mu_R\left(\frac{\lambda_L}{3\bar{\lambda}}\right)\mathcal{L}^{-1}\left(\frac{\bar{\lambda}}{\lambda_L}\right). \tag{25}$$

The modulus $\mu\to\infty$ as $\bar{\lambda}\to\lambda_L$, since $\mathcal{L}^{-1}(z)\to\infty$ as $z\to 1$.

[3]To evaluate $x=\mathcal{L}^{-1}(y)$ for a given y in the range $0<y<1$, one may numerically solve the non-linear equation $f(x)=\mathcal{L}(x)-y=0$ for x. Alternatively, the following approximation for $\mathcal{L}^{-1}(y)$ is useful in the range $0<y<1$:

IF $(0<y<0.84136)$ THEN
$\quad\mathcal{L}^{-1}(y)=1.31446\,\tan(1.58986\,y)+0.91209\,y$
ELSE IF $(0.84136\le y<1)$ THEN
$\quad\mathcal{L}^{-1}(y)=\frac{1}{(1-y)}$
END IF

G. Simple extension

Consider a simple extension deformation defined by

$$\lambda_1=\lambda,\quad \lambda_2=\lambda_3=\lambda^{-1/2},\quad \bar{\lambda}=\frac{1}{\sqrt{3}}\sqrt{\lambda^2+2\,\lambda^{-1}},$$

together with the engineering stresses

$$S_1=S,\quad S_2=S_3=0\,.$$

For this case, using (23)

$$S=\mu\lambda-p\lambda^{-1}, \tag{26}$$
$$0=\mu\lambda^{-1/2}-p\lambda^{1/2}, \tag{27}$$
$$0=\mu\lambda^{-1/2}-p\lambda^{1/2}, \tag{28}$$

leads to

$$p=\mu\,\lambda^{-1},$$

substitution of which in (26) yields that the engineering stress in simple tension is given by

$$\boxed{S=\mu\,\left(\lambda-\lambda^{-2}\right),\qquad \mu=\mu_R\left(\frac{\lambda_L}{3\bar{\lambda}}\right)\mathcal{L}^{-1}\left(\frac{\bar{\lambda}}{\lambda_L}\right).} \tag{29}$$

III. Macroscale tension and compression experiments on PDMS

PDMS is a two part polymer in which a monomer is mixed with a curing agent, degassed and cured. The composition of PDMS is the ratio of monomer to curing agent. The most common composition of PDMS is 10:1, while in multilayer microfluidic devices, compositions of 5:1 and 20:1 are also used.

To span the range of common compositions, the 5:1 and 20:1 compositions were made by mixing the appropriate ratios of monomer to curing agent in a Thinky Hybrid Defoaming Mixer for 3 minutes, and degassing for 5 minutes. The mixture was cast into a 1 mm thick sheet in a pyrex pan, and then cured for eight hours at 80°C. Tension specimens were stamped from the cured sheet with a die conforming to ASTM standard D412-98a. A typical tension specimen is shown in Fig. 2(a). Small black dots (of electrical tape) were applied to the surface of the gage section to allow for optical strain measurements by a non-contacting method.

For the compression experiments, cylindrical specimens that were 3/8 inch diameter and 1/2 inch tall were prepared by casting mixed and degassed 5:1 and 20:1 PDMS into an aluminum mold, and curing at 80°C for 8 hours. A typical compression specimen is shown in Figure 2(b).

Tension and compression experiments were conducted on a Zwick/Roell testing machine using displacement control. Strains in the gauge sections of the specimens, were measured by a non-contacting technique using a

	Avg. μ_R MPa	Range μ_R MPa	Avg. λ_L	Range λ_L
5:1T:	0.34	0.25–0.45	1.24	1.23–1.25
5:1C:	0.31	0.28–0.33	1.44	1.41–1.50
20:1T:	0.15	0.12–0.21	2.06	1.65–2.30
20:1C:	0.11	0.095–0.125	2.38	2.05–3.00

TABLE I

MATERIAL PARAMETERS FIT TO THE MACROSCALE TENSION AND COMPRESSION EXPERIMENTS OF 5:1 AND 20:1 PDMS. NOTE: T STANDS FOR TENSION TESTS, AND C FOR COMPRESSION TESTS. THE RANGES INDICATE THE DEGREE OF SCATTER IN THE SPECIMENS.

CCD camera and image analysis software. The resulting engineering stress versus stretch curves for 5:1 and 20:1 PDMS are shown in Fig. 3.

As expected, the stress-stretch response of PDMS is highly nonlinear, and highly dependent on composition. What is surprising is the amount of scatter in the tension response *of specimens which were nominally identically processed*. The root causes for the substantial variation in the stress-stretch response are still being investigated. The stress-stretch curves for the 10:1 composition (not reported here) are expected to lie between those for the 5:1 and the 20:1 compositions. Tests on the 10:1 composition are still underway, and will be reported when completed.

IV. CALIBRATION OF THE MATERIAL PARAMETERS OF PDMS FROM THE MACROSCALE TENSION AND COMPRESSION EXPERIMENTS

In this section we explore the applicability of the nonlinear rubber-elasticity model summarized in Section II to the stress-stretch response of PDMS determined in Section III. The theoretical stress-stretch curve (29) for simple extension was coded in Matlab, and the values of the two material parameters μ_R and λ_L were adjusted to fit the experimentally-determined macroscale tension and compression engineering stress versus stretch curves. The results of applying (29) to *one* of the engineering stress-stretch curves *for each of the 5:1 and 20:1 compositions* are shown in Figure 4. The fit is very reasonable.[4] The average values of μ_R and λ_L obtained by fitting curves to all the experimental data are shown in Table I.[5]

Although we have taken substantial care in performing our experiments, the significant variations in the material parameters for any one given composition, and also tension versus compression differences, all reflect the current limitations of our material preparation and experimental methods. Work is in progress to improve our experimental techniques.

[4]The data from the compression tests is difficult to interpret due to (a) initial seating effects of the compression platens, (b) friction at the interfaces between the specimen and the platens, and (c) bulging. Appropriate corrections were made to the experimental data to approximately account for these effects.

[5]Note that the magnitude of the material parameter λ_L, the locking stretch, is relative to the effective stretch $\bar{\lambda}$, and not the axial stretch λ.

V. MICROSCALE TENSION EXPERIMENTS ON THIN FILMS OF PDMS

The layers in multi-layer microfluidic devices made from PDMS are approximately 50 μm thick. The deformation and failure behavior of such thin-film PDMS materials is not well-documented.

A mold for casting 50 μm thin films of PDMS was made on a silicon wafer by following the procedure below: (a) SU8-50 photoresist was spun on a silicon wafer at 500 rpm for 10 seconds, and then at 1250 rpm for 30 seconds to build a 50 μm thick layer of the photoresist. (b) The photoresist coated silicon wafer was cured at 65°C for 10 minutes and then at 95°C for 30 minutes. (c) A transparency mask with a pattern of dog-bone shaped tension specimens, Fig.5, was placed on top of the SU8 layer, and the assembly was exposed to UV light for approximately two minutes to set the pattern in the photoresist. (d) The transparency mask was removed and the resulting patterned photoresist was cured at 65°C for 1 minute and then at 95°C for 10 minutes. (e) The SU8 was developed using a wash of propylene glycol methyl ether acetone (PGMEA) for approximately 15 minutes, and then rinsed with isopropyl alcohol and then water.

Samples of PDMS with compositions of 5:1, 10:1 and 20:1 were prepared by mixing the appropriate composition for 1 minute and degassing for 2 minutes in a Thinky Hybrid Defoaming Mixer. The mixed and degassed mixtures of PDMS were carefully poured into different molds, and the excess was carefully removed. The filled molds were cured at 80°C for 8 hours. The thin-film tension specimens of 5:1, 10:1, and 20:1 compositions were then carefully peeled from the molds.

The dimensions of the thin-film tension specimens were measured using a CCD camera and an optical calibration scale. Black paint dots were carefully applied to the gage section of each specimen to allow for optical strain measurements.

To conduct an experiment, a thin-film tension specimen was carefully placed in the grips of a special purpose low-load testing machine developed by Gudlavalleti [8], Fig. 6. The specimen was extended approximately 5 mm at 20 μm/s. Non-contacting strain measurements were performed using a CCD camera and image analysis software. The resulting engineering stress versus stretch curves for thin films of 5:1, 10:1, and 20:1 PDMS are

shown in Fig. 7.[6]

Again, as expected, the stress-stretch response of PDMS is highly nonlinear and strongly dependent on the composition. As before, there is considerable scatter in the response *of specimens which were nominally identically processed*; with the scatter being the largest for the 5:1 composition. The material parameters (μ_R, λ_L) for PDMS were obtained by fitting (29) to the experimental thin-film stress-stretch data. The range of material parameters obtained were: (a) For 5:1, $\mu_R = 0.38 - 0.68$ MPa, and $\lambda_L = 1.16 - 1.22$, (b) For 10:1, $\mu_R = 0.39 - 0.44$ MPa, and $\lambda_L = 1.28 - 1.33$; and (c) For 20:1, $\mu_R = 0.11 - 0.17$ MPa, and $\lambda_L = 1.58 - 2.10$.

Fig. 8 shows a comparison of experimentally-measured versus numerically-fit stress-stretch curves for *representative* thin-film tests on 5:1, 10:1, and 20:1 PDMS. The material parameters used in this figure were: (a) For 5:1, μ_R=0.68 MPa, λ_L=1.2; (b) For 10:1, μ_R=0.44 MPa , λ_L=1.33; (c) For 20:1, μ_R=0.11 MPa, λ_L=1.58. As is clear from this figure, the fit of the constitutive model to *any one set* of the thin-film experimental data is very good.

VI. Application to micro-indentation of PDMS

As a first attempt towards the goal of estimating the non-linear material parameters for PDMS from indentation experiments, we have conducted micro-indentation experiments using a spherical indenter tip, and carried out corresponding numerical simulations to verify how well the numerically-predicted P (load)-h (depth of indentation) curves compare with the corresponding experimental measurements.

The micro-indentation experiments were conducted on an apparatus developed by Gearing [9], using a 450 μm radius spherical indenter tip, under load-control. The experimentally-measured P (load)-h (depth of indentation) curves for the 5:1 and 20:1 compositions are shown in Fig. 9.

The PDMS to be indented was modelled using an axisymmetric mesh, with a radius of 4 mm and a height of 2 mm, using 2940 ABAQUS-CAX4R elements, Fig. 10; the mesh density was higher near the indenter tip where most of the deformation was expected to occur. The spherical indenter tip was modelled using an axisymmetric rigid-surface with a radius of 450 μm . The average material parameters from the *macroscale compression experiments*: (a)For 5:1, μ_R=0.31 MPa , λ_L=1.44; and (b) For 20:1, μ_R=0.11 MPa, λ_L=2.38, were used in the numerical simulations.

[6]The elastomer PDMS exhibits some softening, so each specimen was conditioned through 2-3 cycles of straining to obtain the equilibrium deformation behavior of each film.

The P-h curves predicted by the simulation are compared against the experimental results in Fig. 11. The predicted results are in reasonably good agreement for the 5:1 composition, with the simulation lying in the middle of the range of the experimental P-h curves. The predicted results for the 20:1 composition lie on the softer side of the experimental P-h curves.

VII. Conclusions

Accurate and reliable design, manufacture, and operation of microfluidic devices made from PDMS require a detailed characterization of the deformation and failure behavior of PDMS. This study represents a reasonable first-attempt towards this goal.

Future work will address: (i) refining our specimen preparation and testing techniques; (ii) modelling the tearing behavior of PDMS; (iii) modelling the interfacial decohesion of PDMS from a substrate to facilitate analysis of demolding operations; (iv) optimizing the geometries of the device components, such as layer thicknesses and channel dimensions; (v) optimizing the flow characteristics within the channels; and (vi) specifying safe operating parameters to prevent interface-decohesion and fatigue failures, so that the devices properly and reliably serve their intended functions.

Acknowledgment

This work was supported by the Singapore MIT Alliance. The help of T. Thorsen and his group in specimen preparation is gratefully acknowledged.

References

[1] J. C. Mcdonald and G. M. Whitesides, "Poly(dimethylsiloxane) as a material for fabricating microfluidic devices," *Accounts of Chemical Research*, vol. 35, pp. 491–499, 2002.

[2] Y. Xia and G. M. Whitesides, "Soft lithography," *Angew. Chem. Int. Ed.*, vol. 37, pp. 550–575, 1998.

[3] J. C. Love, J. R. Anderson, and G. M. Whitesides, "Fabrication of three-dimensional microfluidic systems by soft lithography," *MRS Bulletin*, vol. July, pp. 523–528, 2001.

[4] M. A. Unger, H. P. Chou, T. Thorsen, A. Scherer, and S. Quake, "Monolithic micro fabricated valves and pumps by multilayer soft lithography," *Science*, vol. 288, pp. 113–116, 2000.

[5] E. M. Arruda and M. C. Boyce, "A three-dimensional constitutive model for the large stretch behavior of rubber elastic materials." *Journal of the Mechanics and Physics of Solids*, vol. 41, pp. 389–412, 1993.

[6] L. Anand, "A constitutive model for compressible elastomeric solids," *Computational Mechanics*, vol. 18, pp. 339–352, 1996.

[7] ABAQUS, Inc., "ABAQUS Reference Manuals," Pawtucket, RI, 2004.

[8] S. Gudlavaletti, "Mechanical testing of solid materials at the micro-scale," *MS Thesis, Massachusetts Institute of Technology*, 2002.

[9] B. P. Gearing, "Constitutive equations and failure criteria for amorphous polymeric solids," Ph.D. dissertation, Massachusetts Institute of Technology, 2002.

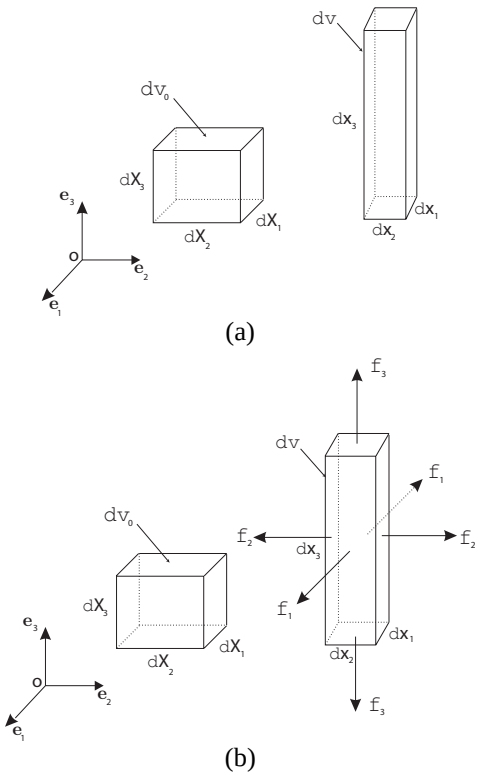

Fig. 1. (a) Schematic of undeformed and deformed configurations. (b) Schematic showing forces in the deformed configuration.

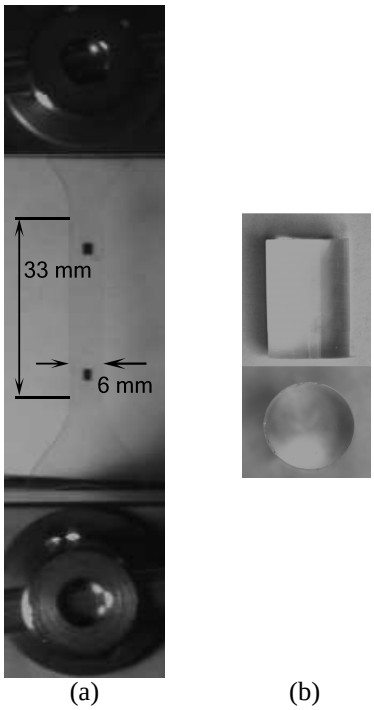

Fig. 2. (a) Macroscale tension specimen. (b) Macroscale compression specimen, 1/2 inch tall, 3/8 inch diameter.

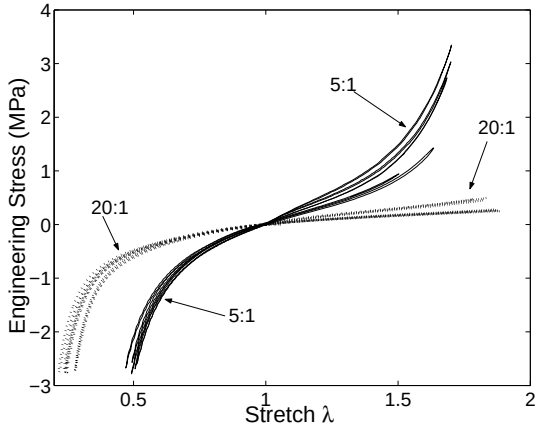

Fig. 3. Macroscale engineering stress versus stretch curves for 5:1 and 20:1 PDMS in tension and compression.

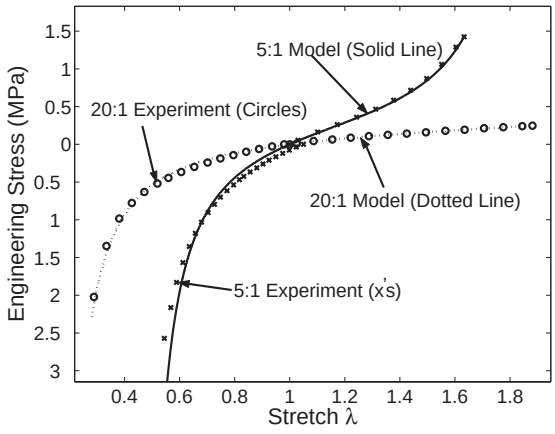

Fig. 4. Comparison of the fit of the model with the experimental data, for engineering stress versus stretch curves from representative macroscale specimens for 5:1 and 20:1 PDMS. Material parameters used were μ_R=0.25 MPa, λ_L=1.238 for 5:1, and μ_R=0.115 MPa, λ_L=2.2 for 20:1.

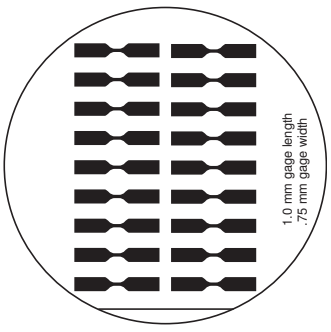

Fig. 5. Transparency mask design for thin film dog-bone specimens with a 1 mm gage-length and 0.75 mm gage-width.

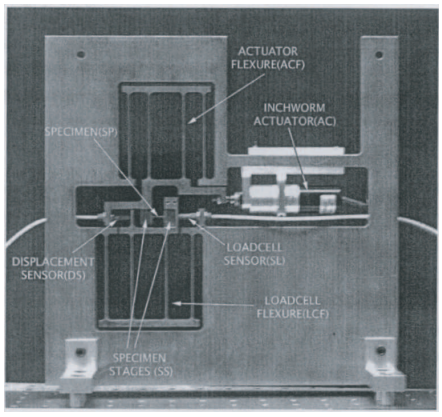

Fig. 6. Small scale tension testing machine [8].

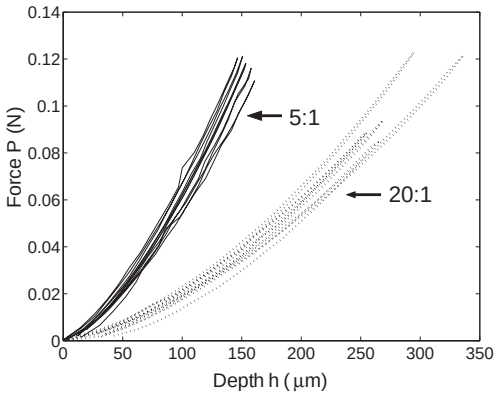

Fig. 9. P-h curves form micro-experiments on 5:1 and 20:1 PDMS.

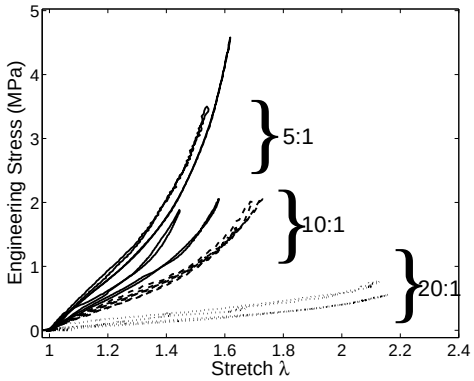

Fig. 7. Stress-stretch curves from thin-film tension tests on 5:1, 10:1, and 20:1 PDMS

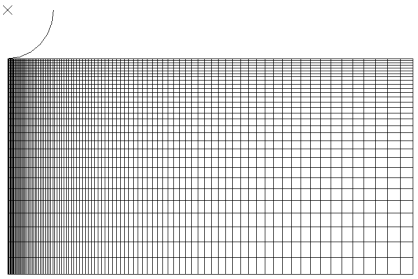

Fig. 10. Finite element mesh used to simulate micro-indentation experiments.

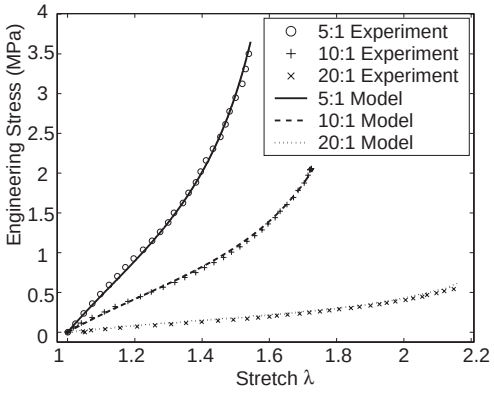

Fig. 8. Comparison of experimentally-measured versus numerically-fit stress-stretch curves from representative thin-film tension tests on 5:1, 10:1, and 20:1 PDMS. Material parameters used were: (a) For 5:1, μ_R=0.68 MPa and λ_L=1.2; (b) For 10:1, μ_R=0.44 MPa and λ_L=1.33; (c) For 20:1 , μ_R=0.11 MPa and λ_L=1.58.

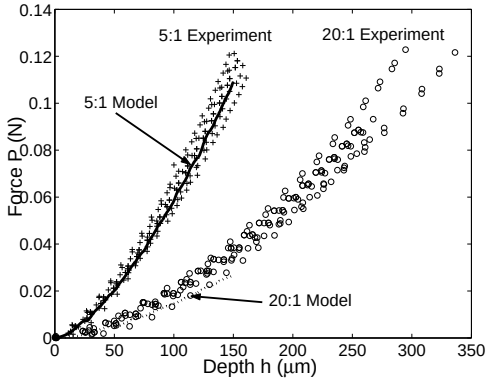

Fig. 11. Comparison of simulated and experimental P-h curves for of 5:1 and 20:1 PDMS.